Journal of Power Sources 196 (2011) 1279–1294

Contents lists available at ScienceDirect

Journal of Power Sources

journal homepage: www.elsevier.com/locate/jpowsour

Microstructure degradation of cermet anodes for solid oxide fuel cells: Quantification of nickel grain growth in dry and in humid atmospheres

L. Holzer[a,*], B. Iwanschitz[b], Th. Hocker[c], B. Münch[a], M. Prestat[a], D. Wiedenmann[a], U. Vogt[a], P. Holtappels[a], J. Sfeir[b], A. Mai[b], Th. Graule[a]

[a] EMPA Materials Science and Technology, Laboratory for High Performance Ceramics, Ueberlandstrasse 129, CH-8600 Dübendorf, Switzerland
[b] Hexis Ltd., Zum Park 5, CH-8404 Winterthur, Switzerland
[c] ZHAW Zürich University of Applied Sciences, Institute of Computational Physics, CH-8401 Winterthur, Switzerland

ARTICLE INFO

Article history:
Received 16 June 2010
Received in revised form 29 July 2010
Accepted 10 August 2010
Available online 17 August 2010

Keywords:
Ostwald ripening
Nickel coarsening
Anode degradation
Particle size distribution (PSD)
Microstructure analysis
Solid oxide fuel cell (SOFC)

ABSTRACT

The effects of compositional and environmental parameters on the kinetics of microstructural degradation are investigated for porous Ni/CGO anodes in solid oxide fuel cells (SOFC). Improved methodologies of SEM-imaging, segmentation and object recognition are described which enable a precise quantification of nickel grain growth over time. Due to these methodological improvements the grain growth can be described precisely with a standard deviation of only 5–15 nm for each time step.

In humid atmosphere (60 vol.% H_2O, 40% N_2/H_2) the growth rates of nickel are very high (up to 140%/100 h) during the initial period (<200 h). At longer exposure time (>1000 h) the growth rates decrease significantly to nearly 0%/100 h. In contrast, under dry conditions (97 vol.% N_2, 3 vol.% H_2) the growth rates during the initial period are much lower (ca. 1%/100 h) but they do not decrease over a period of 2000 h.

In addition to the humidity factor there are other environmental and compositional parameters which have a strong influence on the kinetics of the microstructural degradation. The nickel coarsening is strongly depending on the gas flow rate. Also the initial microstructures and the anode compositions have a big effect on the degradation kinetics. Thereby small average grain sizes, wide distribution of particle size and high contents of nickel lead to higher coarsening and degradation rates.

Whereas the nickel coarsening appears to be the dominant degradation mechanism during the initial period (<200 h) other degradation phenomena become more important during long exposure time (>1000 h) in humidified gas. Thereby the evaporation of volatile nickel species may lead to a local increase of the Ni/CGO ratio. Due to the surface wetting of CGO a continuous layer tends to form on the surface of the nickel grains which prevents further grain growth and evaporation of nickel. These phenomena lead to a microstructural reorganization between 1000 and 2300 h of exposure. This complex pattern of degradation phenomena also leads to a change of the amount of active microstructural sites that are important for catalytic reactions at the pore-nickel interfaces and for electrochemical reactions at the triple phase boundaries (TPB).

1. Introduction

Solid oxide fuel cells represent a promising technology for highly efficient energy conversion e.g. of natural gas, syn-gas and hydrogen. However due to the harsh operating conditions, which include high temperatures (up to 1000 °C) and variable gas compositions (e.g. changing humidity and impurities), the conversion efficiency decreases steadily with time. Understanding the interplay between the loss of electrochemical performance and the degradation mechanisms on a microscopic scale is important for the successful improvement of the solid oxide fuel cell (SOFC) durability.

Significant microstructural changes are especially reported for standard Ni-cermet anodes [1]. The degradation mechanisms of nickel-based cermet anodes include different phenomena such as coking [2], poisoning by fuel impurities [3], Red Ox cycling [4–6] and general microstructural alteration [7]. With respect to the microstructural degradation, the grain growth of nickel is usually considered as the most prominent feature [7–10]. The grain growth of nickel is also set into direct relationship with the corresponding reduction of the triple phase boundary length (TPB_L) [11]. Furthermore, the TPB_L is interpreted as the electrochemically active area in the composite Ni/YSZ anodes where fuel oxidation and charge

* Corresponding author. Tel.: +41 44 823 44 90; fax: +41 44 823 40 23.
E-mail address: Lorenz.holzer@empa.ch (L. Holzer).

0378-7753/$ – see front matter © 2010 Elsevier B.V. All rights reserved.
doi:10.1016/j.jpowsour.2010.08.017

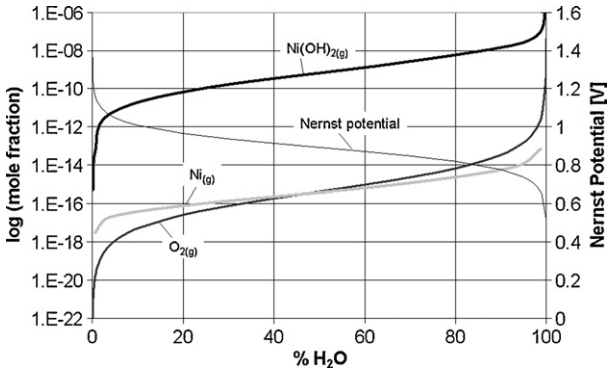

Fig. 1. Thermodynamic data from literature [20] for two different nickel species in a gas mixture of $H_{2(g)} + H_2O_{(g)}$ in equilibrium with metallic nickel at 950 °C and 1 atm. The partial pressure of volatile $Ni(OH)_{2(g)}$ is six orders of magnitude higher than that of pure $Ni_{(g)}$. Note that the concentration of volatile $Ni(OH)_{2(g)}$ is not linearly correlated to P $H_2O_{(g)}$, but it is proportional to the activity of $O_{2(g)}$. The Nernst-potential is calculated for an SOFC with oxygen pressure of 0.21 [bar] on the cathode side.

transfer reactions take place [12–15]. From this relationship it can be deduced that the electrochemical performance of the anode is degrading mainly due to the coarsening of nickel and due to the associated decrease of the TPB_L [16]. Nevertheless the relationship between decreasing conversion efficiency with synchronous grain growth of nickel was not yet proven rigorously. So far, no study was found which has successfully and systematically quantified both, the kinetics of nickel coarsening over time and the contemporaneous decrease of the electrode performance.

In the present study we are thus focusing on the quantitative description of the grain growth in composite Ni/CGO anodes. For this purpose we have improved the methodologies for microstructural analysis by means of SEM and image analysis techniques. The reproducibility of these methodologies is first tested for a set of pristine nickel cermet anode samples and then the methods are applied for the quantification of grain growth in dry and in humid gas for two different anode compositions (i.e. anode with two layers of different compositions). The quantitative results are combined with additional qualitative observations which lead to a more thorough description of the complex degradation phenomena in Ni-based cermet anodes. For the interpretation of these complex degradation phenomena we take into account the potential mechanisms of grain growth and the previous investigations on nickel coarsening which are briefly reviewed in the following sections.

1.1. Mechanisms of nickel grain growth

Coarsening of the nickel phase is a prominent feature of microstructural degradation in SOFC anodes. It is usually attributed to some kind of Ostwald ripening [9,10,17–19]. Thereby, two different scenarios are discussed as potential underlying mechanisms for the Ostwald ripening phenomena: (A) transport of volatile nickel species via the gas phase (i.e. evaporation and precipitation) [20] and (B) diffusion of vacancies, driven by different grain sizes and surface curvatures [21].

(A) *Transport of nickel in the gas phase*: Several authors have observed local enrichment of nickel (e.g. within cracks) and also considerable local depletion of the nickel content in cermet anodes [18,20]. These phenomena were interpreted as evidence for evaporation and re-precipitation due to variable oxygen activities within the anode layer. At equilibrium with a humid gas, the volatilization of nickel is dependent on the gas pressures of each nickel species. The thermodynamic data from literature indicates that $Ni(OH)_{2(g)}$ is the most volatile species in a gas mixture of H_2 and H_2O [20,22]. As shown in Fig. 1 the partial pressure of $Ni(OH)_{2(g)}$ is six orders of magnitude higher than that of pure $Ni_{(g)}$. According to the thermodynamic data, the volatilization of pure nickel at 950 °C under dry conditions is very low, whereas even at low H_2O concentrations the formation of $Ni(OH)_2$ leads to much stronger evaporation. Thus, when starting with a dry gas of $H_{2(g)}$ the partial pressure of Ni (i.e. the sum of all gaseous Ni-species) increases rapidly upon the addition of small quantities of water vapour (i.e. 1–2% $H_2O_{(g)}$). In contrast, for gas mixtures with higher water contents (i.e. between 10 and 90% $H_2O_{(g)}$) the partial pressure of $Ni(OH)_2$ is less sensitive to changes of the $H_2O_{(g)}$ concentration. The observed coarsening of nickel in SOFC anodes may thus be caused by local variations of the gas composition which leads to selective evaporation (of small grains preferentially) and to re-precipitation on the surface of larger grains [20].

(B) *Nickel coarsening by diffusion of vacancies*: A very different perception of nickel grain growth was presented in a so-called 'two particle model' [21]. In this model the driving force for nickel grain growth is explained by the different curvatures of neighbouring particles. According to the Kelvin equation [23], gas pressures at equilibrium inversely relate to the particle radii. This relationship also indicates higher vacancy concentrations for smaller particles. The resulting concentration gradients between neighbouring particles with different radii induce diffusive fluxes of vacancies. For this type of Ostwald ripening it was concluded that the different curvatures and the coefficient of vacancy surface diffusion represent the main factors which control the growth kinetics. According to this model the driving force for grain growth of nickel is higher for microstructures with wider Ni-particle size distributions (PSD) but it will decrease during the ongoing coarsening.

It has to be mentioned that this model does not take into account surface diffusion of nickel and the effect of humidity on the diffusion coefficient. However it is well known from steam-reforming nickel catalysts that the surface diffusion of Ni is strongly enhanced by humidity (i.e. diffusion of Ni-hydroxide complexes) which may play an important role for the grain growth of nickel in SOFC anodes [24,25].

In summary, at least two different mechanisms may be responsible for nickel grain growth. The kinetics of both mechanisms is strongly accelerated by the presence of water in the gas phase.

1.2. Microscopic description of nickel grain growth

The quantitative description of grain growth under controlled environmental conditions may give an indication on the rate controlling parameters in Ni-YSZ or in Ni-CGO anodes. Unfortunately, in literature only a few investigations can be found describing the grain growth of nickel on a quantitative level. This literature data is plotted in Fig. 2 and it is briefly discussed in the following section:

- Simwonis et al. [26] have measured nickel grain growth on samples which were exposed to a humid gas environment (3% H_2O) at 1000 °C for up to 4000 h. During the entire period the coarsening was relatively slow. However there is a clear tendency of decreasing growth rates with increasing time. This experimental growth curve could be simulated reasonably well based on the mentioned 'two particle model' [21] which is driven by different vacancy concentrations. It is important to note, that the simulation had to be performed with a very low surface diffusion coefficient of 10^{-13} [m s^{-2}] in order to reproduce the measured, slow growth rates [26].
- In contrast, Jiang [8] reported much faster growth rates of nickel under similar conditions (1000 °C/3% H_2O). The authors analyzed the particle size of nickel on a fractured cross-section. Thereby the growth rates were particularly high during the early periods of 200–800 h and they decreased at longer times. The anode composition was also found to have a strong effect on

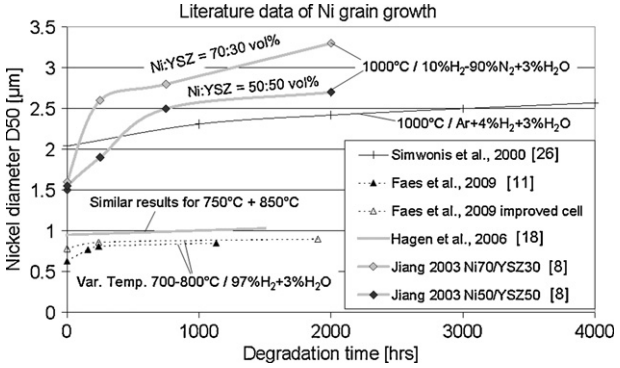

Fig. 2. Nickel grain growth over time (data from literature). Note that these degradation experiments are performed under different operating conditions, with different cell types (i.e. anode or electrolyte supported) and with different microstructures (i.e. different compositions and different initial particle sizes). These differences must be taken into account when comparing the underlying growth kinetics.

nickel coarsening: Faster growth rates were measured for nickel-rich anodes (70 vol.% Ni/30 vol.% YSZ) in comparison to a slower degradation which was observed in anodes with higher ceramic content (50% Ni/50% YSZ).

- Hagen et al. [18] investigated microstructural degradation of Ni-YSZ anodes which were exposed to 750 °C at 0.75 A cm^{-2} and to 850 °C at 1.9 A cm^{-2}. Different current loads were found to have no effect. In their experimental setup the average nickel grain size did not increase markedly, but widening of the particle size distributions were observed. Nevertheless, considerable local reduction of the nickel volume fraction was reported (up to 40%). This compositional change was attributed to the volatilization of nickel hydroxides in the hydrous environment of the anode.
- Recently, Faes et al. [11] measured grain growth in two different types of anode supported cells, one with a fine grained microstructure and the other with a coarser grained microstructure. The gas contained 3% H_2O and the temperatures varied between 700 and 800 °C. In the fine grained anode the growth rate was much higher during the first 240 h compared to the longer exposure time. In contrast, the coarse grained microstructure was much more stable at the beginning of the exposure. The measured evolution of the particle sizes could be nicely fitted with a so-called 'charging capacitor model'. In this model the growth curves asymptotically approach a maximum nickel grain size that is reached after ca. 1000 h.

In summary, the above mentioned studies reveal a puzzling picture with respect to the impact of different environmental and compositional parameters. Most studies indicate that grain growth of nickel tends to be faster during an initial period of approximately 200 h and afterwards the growth rates decrease significantly. However, very different growth curves were obtained for example by Jiang [8] and by Simwonis et al. [26] under very similar experimental conditions (1000 °C, 3% H_2O). From the studies in literature it is also not clear to what extent the growth kinetics are affected by the water contents in the gas phase or by the temperature. Thus, the impact of these parameters can neither be quantified nor can they be weighted according to their severity. For this purpose the data from literature is too scarce and does not provide an unambiguous picture.

One reason for these apparently contradicting findings in literature might be related to the methodological uncertainty of particle size measurements. In particular, the geometrical model underlying the particle size measurement may strongly influence the results of a size measurement [27], as will be discussed later. Because different measurement techniques are applied by different authors, this effect must be considered when comparing the different data sets from literature with each other. In order to reduce such uncertainties and to increase the methodological reliability we have carefully evaluated our own quantification procedure in the present study. The improved methods are then applied for two degradation experiments with porous nickel/CGO anodes. Thereby, nickel grain growth is investigated at 950 °C first in a dry environment (experiment A) and then in a humid environment (experiment B). Since the anodes are screen printed in two layers with different compositions the influence of different nickel and ceramic contents on the growth kinetics is investigated in the two experiments. In addition to the quantitative description of the grain growth it is also of interest to unravel which type of mechanism is dominating the degradation kinetics under dry and humid conditions. For this purpose qualitative microscopic observations are also taken into account.

2. Experimental

As shown in Fig. 3 the experimental procedure includes fabrication of anode layers, their reduction at 950 °C and subsequent degradation experiments. The procedure for microstructure analysis is described in Section 3 below.

Ni/CGO anode powders from Praxair Specialty Ceramics were mixed with a terpineol based solution in a ball mill. The pastes are composed of 50 wt% NiO and 50 wt% CGO (anode 1) and of 70 wt% NiO and 30 wt% CGO (anode 2). The slurries were screen printed in two layers on a 3YSZ electrolyte (Nippon Shokubai). Anode 1 is facing the electrolyte, whereas anode 2 is a current collecting layer on top of it. The anodes were sintered at 1350 °C for 4 h. By taking into

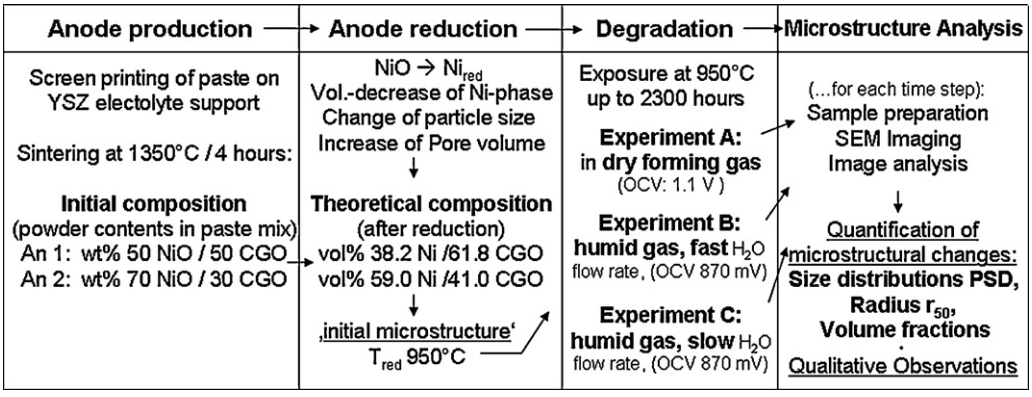

Fig. 3. Summary of experimental work flow for anode production, reduction, degradation testing and microstructural analysis. An 1 = anode layer 1, close to electrolyte, An 2 = anode layer 2, close to gas channel and metallic interconnector.

Table 1
Gas compositions and gas flow rates in degradation experiments A, B and C.

	Flow of H_2	Flow of N_2	Flow of H_2O	Vol.% N_2/H_2	Nernst-potential	Vol.% H_2O
Experiment A	6 ml min^{-1}	200 ml min^{-1}	0.0 ml h^{-1}	97.5/2.5	1.10 V	~2
Experiment B	29 ml min^{-1}	200 ml min^{-1}	6.0 ml h^{-1}	85.5/14.5	0.87 V	~60
Experiment C	6 ml min^{-1}	200 ml min^{-1}	0.8 ml h^{-1}	97.5/2.5	0.87 V	~60

account the density change of the nickel phase during reduction, the volume fractions of the solid phases in the reduced anodes can be calculated. The theoretical composition of the reduced anode layer 1 is 38.2 vol.% Ni and 61.8 vol.% CGO. In the reduced anode layer 2 the theoretical composition is 59 vol.% Ni and 41 vol.% CGO.

Three different degradation experiments were performed in a tube furnace inside an aluminium-oxide tube: Experiment A: dry gas, experiment B: humid gas, high flow rate and experiment C: humid gas, low H_2O flow rate (see Table 1). For all three experiments, small pieces of the anode/electrolyte half cells (~0.25 cm^2) were placed on an aluminium-oxide sample holder. The temperature was measured directly on the sample holder using a type S thermocouple. A Pt/YSZ/Pt sensor was used to measure the Nernst-potential. Hydrogen and nitrogen were mixed with mass flow controllers and a precision evaporator from Bronkhorst (Controlled Evaporator Mixer) was used to humidify the gas. All mass flow controllers were calibrated before the experiment. The furnace was heated up and cooled down with a rate of 3 °C min^{-1}. For the first reduction the samples were heated to the reduction temperature (950 °C) in oxidizing atmosphere. Afterwards the tube was flushed with N_2 for 2 h followed by the introduction of hydrogen for reduction. The reduction at 950 °C was considered to be completed after 1 h of hydrogen flow. This is considered to be the initial data point at 0 h. During the aging experiments, pieces of the anode/electrolyte half cells were removed at different exposure times from the furnace. For this purpose the furnace was cooled down and reheated under reducing atmosphere.

The influence of different water vapour concentrations on the microstructural degradation was investigated in experiments A and B. In experiment A the anodes were exposed to a dry forming gas for up to 2000 h (Nernst-potential: 1.1 V). In experiment B the gas mixture consisted of forming gas and additional water vapour (Nernst-potential: 0.87 V). The samples were exposed for up to 2300 h. In experiment C the samples were exposed to the same gas composition as in experiment B, but at a lower H_2O mass flow. The gas compositions and flow rates for experiments A, B and C are listed in Table 1.

3. Microstructure analysis

Microstructural analysis for quantification of particle size distributions consists of four main steps: (a) sample preparation, (b) imaging, (c) segmentation and (d) quantification of microstructural parameters. Each of these steps may introduce considerable analytical uncertainties and/or errors. In this study we have carefully evaluated potential sources of uncertainty and error in order to improve reliability of our methodological procedure:

3.1. Sample preparation

For quantitative analysis from 2D images it is crucial to produce perfectly flat cross-sections. For this purpose the pores are infiltrated with a resin (4 parts Araldite BY158 mixed with 1 part Aradur hardener/12 h at 80 °C) followed by mechanical grinding with SiC paper, polishing and finally coating with a thin carbon layer of a few nm. For samples which were exposed for more than 1000 h to a humid environment (experiment B) mechanical grinding and polishing produced irregular surfaces which resulted in artificially high porosities and apparently large pores. Perfectly flat cross-sections of these samples could be produced with a focused ion beam (FIB) machine. The resulting quantitative results match well with the extrapolation of the growth curves from younger samples (Fig. 11). Hence, with the FIB technique [28,29] the preparation artifacts in delicate and brittle samples can be avoided.

3.2. SEM imaging

In order to obtain precise and reproducible results, the SEM images must accomplish some basic requirements such as constant image values, sufficient resolution, representative window size and unambiguous contrast:

- Constant image grey scales and contrast:
  Reliable automated identification of the different phases is only possible with stable image values. This means that the same phases should always be represented by the same grey scale values during the entire measurement campaign. For this purpose the basic imaging parameters (accelerating voltage, beam current, blend, spot size and detection mode) must be adjusted accordingly in order to match with the empirical grey scale values of each phase. In the present study the imaging was performed with a FEI Nova NanoSEM230 equipped with a solid state BSE detector. The acceleration voltage was 5 kV. Spot size (3.5–4.5), contrast and brightness were adjusted in order to obtain reproducible grey scale values (Note: for sufficient contrast in Ni/YSZ anodes low voltage SEM imaging would be required [30]).
- Resolution (small pixel size) vs. representativity (large image window):
  Usually there are conflicting requirements between a high resolution that is necessary for the identification of the smallest objects in the microstructure and a large image window which is needed for a statistical representation of the largest objects. Hence, resolution and image size must be adapted according to the particle size distribution in the sample. In the present study these two parameters were evaluated empirically for the initial microstructure in anodes that are reduced at 950 °C.

For the evaluation of a sufficient pixel resolution the image window was kept at constant size (30 μm width) and the pixel matrix was varied in order to obtain different magnifications. By comparing the PSDs from different resolutions it was found that up to a pixel size of 35 nm the results are nearly identical. Thus, for this anode microstructure higher magnifications with pixel dimensions smaller than 35 nm do not provide additional information for the measurement of particle size distributions. However, if imaging is performed with pixel sizes larger than 35 nm then the smallest particles with radii <100 nm cannot be quantified correctly.

For the evaluation of a suitable image window size the pixel resolution was kept constant at 20 nm. By varying the size of the image window and by comparing the resulting PSDs it was found that images smaller than 400 μm^2 (20 μm width) were not representative. Instead, local heterogeneities became prominent in the PSD analyses. In contrast nearly identical PSDs could be obtained with image windows larger than 400 μm^2 which documents the good reproducibility.

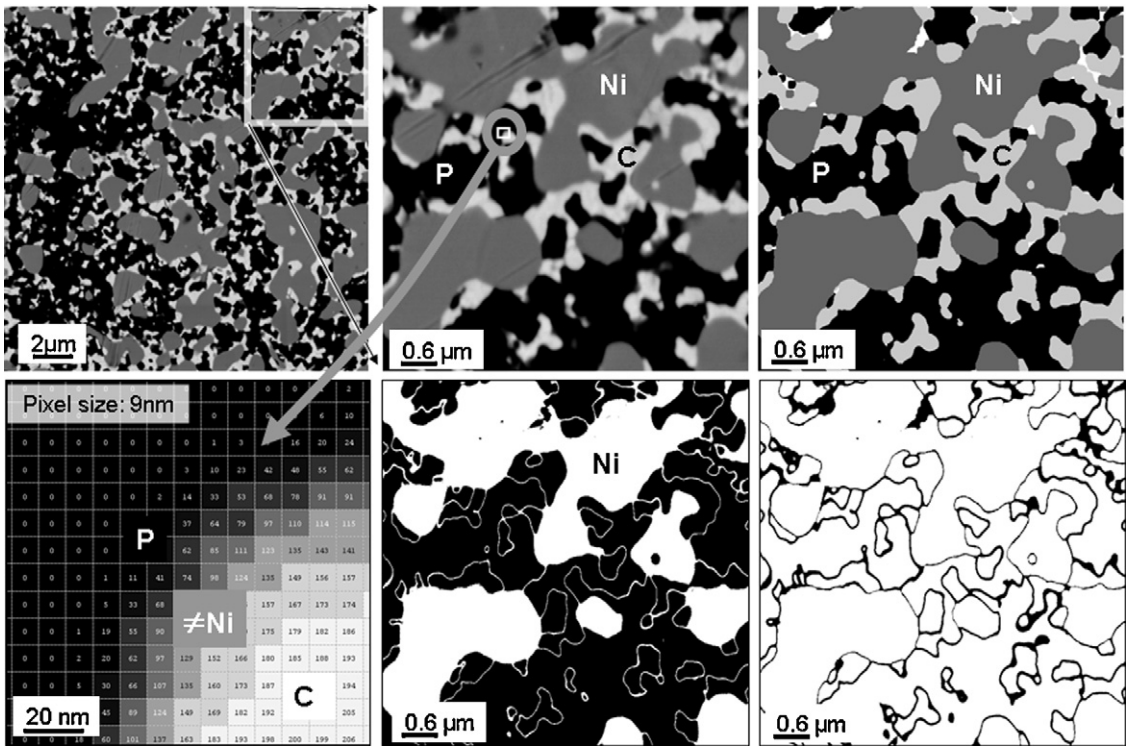

Fig. 4. Illustration of the segmentation procedure. The phases in the top row are Ni = nickel (dark grey), C = CGO (bright grey), P = pore (black), 'non-assigned rest' (white); Top left: original BSE image (20 µm image width, 9 nm pixel size); Top centre: 'zoom-in' from original grey scale image; Top right: labelled image after final segmentation; Bottom left: 'zoom-in' at interface between pore (P) and CGO (C); Bottom centre: binary image after threshold segmentation of nickel (white). Note that the nickel phase apparently includes the transition zones between pore and CGO; Bottom right: Isolated transition zones (black) after conservative threshold segmentation represent 15% of the total image. The pixels of these transition zones are redistributed to the neighbouring phases by using an asymmetric region growing process which results in a labelled image (top right).

In summary it can be concluded that the 'initial microstructure' of our Ni/CGO anode material (reduced at 950 °C) can be characterized in a precise and reproducible way based on a resolution with maximum pixel size of 30–35 nm and with an image window of at least 400 µm^2 (i.e. image width of 20 µm). Proof of a good reproducibility with our procedure is documented later in Fig. 6 which represents a series of PSD measurements from different samples with the same composition (i.e. initial anode microstructure before degradation).

3.3. Segmentation

A major uncertainty for quantitative microstructure analysis is related to the excitation volume of backscattered electrons (BSE). The depth penetration of the primary electron beam and the size of the excitation volume depend on material density (atomic number) and on accelerating voltage. In order to reduce the excitation volume low voltage imaging would be beneficial. However, for reasonable contrast with conventional solid state BSE detectors a minimum accelerating voltage of 5 kV is required which limits the effective resolution. This is illustrated in Fig. 4 (bottom left). At high magnification the interface between pore and CGO is not represented by a sharp line but it is rather characterized by a gradual change of grey scales. At 5 kV this grey 'transition zone' is 40–70 nm wide (i.e. 5–7 pixels at 9 nm resolution). If segmentation of the nickel phase is performed with a simple grey scale threshold value, then the transition zones between CGO (white) and pores (black) are erroneously attributed to the nickel phase (Fig. 4, bottom centre). In our fine structured material the transition zones at the phase boundaries represent up to 15% of the total image area (see black areas in Fig. 4, bottom right). The unambiguous assignment of the pixels in these transition zones to the neighbouring phases is thus a prerequisite for reliable and precise quantification. Therefore in the present study a segmentation procedure was developed which allows the identification of the phase boundaries based on geometrical criteria instead of the grey scale values. In our procedure the 'core regions' of each phase are first identified by applying 'conservative' grey scale threshold values. After this step the pixels in the transition zones are not yet attributed to any phase (black pixels in Fig. 4, bottom right). In a second step, these pixels from the transition zones are then 'redistributed' to the neighbouring phases by an asymmetric region growing process. The algorithm for the redistribution takes into account the asymmetry of the excitation volume at the phase boundary which is caused due to the different atomic numbers of epoxy (pores), CGO and nickel. Additional input parameters for the redistribution are the accelerating voltage and the pixel resolution, because they control the width of the transition zones. Each phase is then labelled with a characteristic grey value (Fig. 4, top right). In these labelled images the phase boundaries are perfectly sharp. A small number of pixels ($\leq$1%) cannot be attributed in this way. Usually these image defects are related to imperfect sample surfaces (e.g. scratches). These 'non-assigned' pixels are labelled in white (top right).

3.4. Quantitative image analysis: different geometrical concepts for phase size distribution (PSD)

From the labelled images various microstructural parameters can be determined for each phase. For the study of microstructural degradation the time dependent changes of phase size distributions (PSD) and the associated average radii (r_{50}) are of primary interest. For the determination of phase size distributions different methods have been proposed in literature, such as the chord length distribution function [31,32], the ray shooting method [33], the intercept

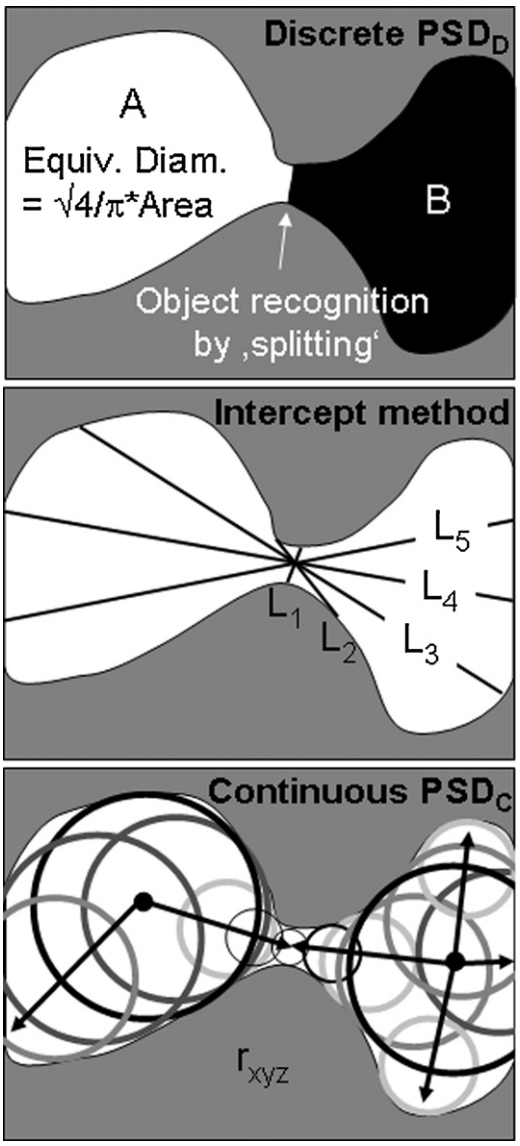

Fig. 5. Illustration of geometrical principles which are inherent to different types of phase size distribution. Each PSD method is based on a different definition for 'object size'. Top: Discrete PSD_D: The particle size is defined as area (2D) or volume (3D) equivalent diameter. Networked microstructures have to be split into discrete objects which may introduce significant uncertainties. Middle: Intercept method: The PSDs reflect the probabilities of different intercept lengths based on randomly oriented lines. For 2D-analysis stereological correction is required which is ill defined for complex particle shapes. Bottom: The continuous PSD_C [27] is based on an algorithm which measures the area (2D) or volume (3D) that can be covered with a circle or sphere of a given radius. By incrementally reducing the radius increasingly larger areas (volumes) can be occupied. In this sense the continuous PSD measurement also represents the simulation of a pressure induced intrusion with a poorly wetting fluid (e.g. mercury intrusion). Neither the recognition of discrete objects nor stereological corrections are required for the continuous PSD method.

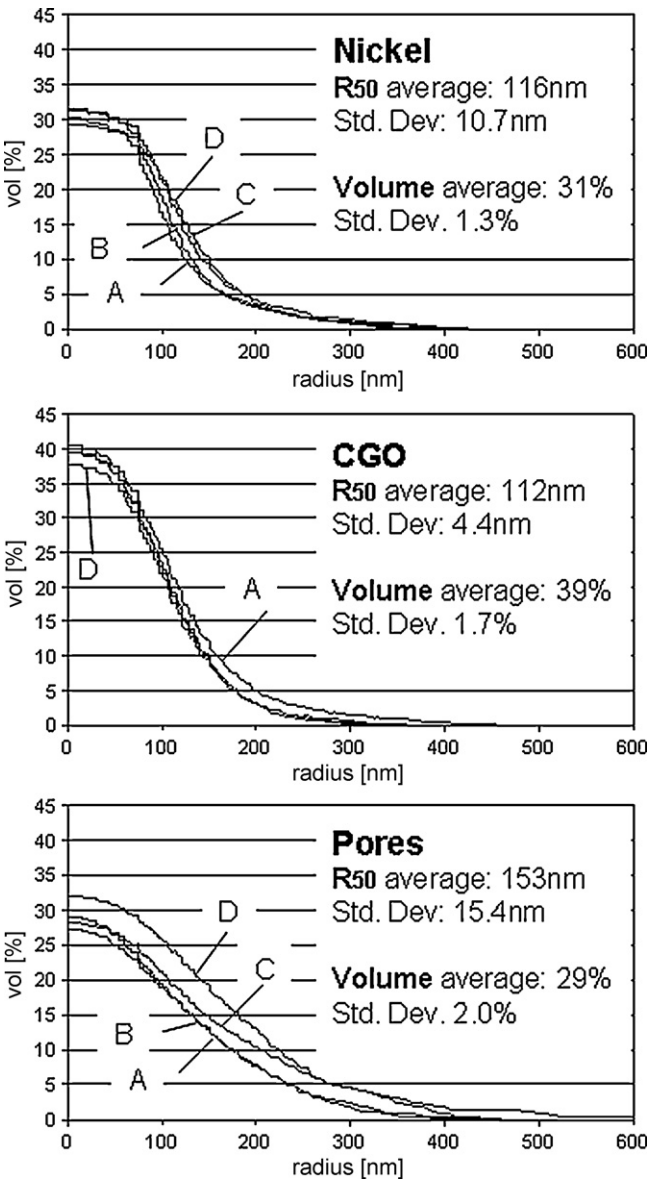

Fig. 6. Continuous PSD_C measurements from four different samples of the same Ni/CGO material. The standard deviations of the r_{50} radii are between 4 and 16 nm, which illustrates the good reproducibility.

method [11], the discrete phase size distribution PSD_D [34,35] and the continuous phase size distribution PSD_C [27]. In this context it is important to note that these methods may result in very different PSD curves for the same image, because each of these methods is based on a different geometrical definition for the 'object size' [36]. In order to identify the most suitable PSD method, the different geometrical principles of the PSD methods are discussed in the following sections.

The measurement of discrete PSD_D (Fig. 5, top) is based on the perception of distinct objects and for each of these the area (in 2D) or the volume (in 3D) is measured. The 'object size' is then defined as the diameter of a circle (sphere in 3D) with equivalent area (volume in 3D). A major challenge for the discrete PSD_D method is the reliable recognition of individual objects. The object recognition is particularly difficult if the percolating phases form networked microstructures which is usually the case for all three phases (Ni, CGO and Pore) in SOFC anodes. For the recognition of discrete objects in networked microstructures a special algorithm was introduced, which splits the continuous network into distinct particles [34]. The splitting, which defines artificial particle–particle interfaces at concave bottle necks, requires 3D data from high resolution (FIB) tomography [35,37]. If the discrete PSD_D is measured from 2D images a stereological correction procedure has to be applied. However for complex particle shapes the splitting itself and also the stereological correction are ill defined, which introduces significant uncertainties.

A very different type of size distribution includes a group of similar techniques such as the intercept, chord length and ray shooting methods. This type of PSD measurement is most frequently used in the study of SOFC microstructures (e.g. [26,11]).

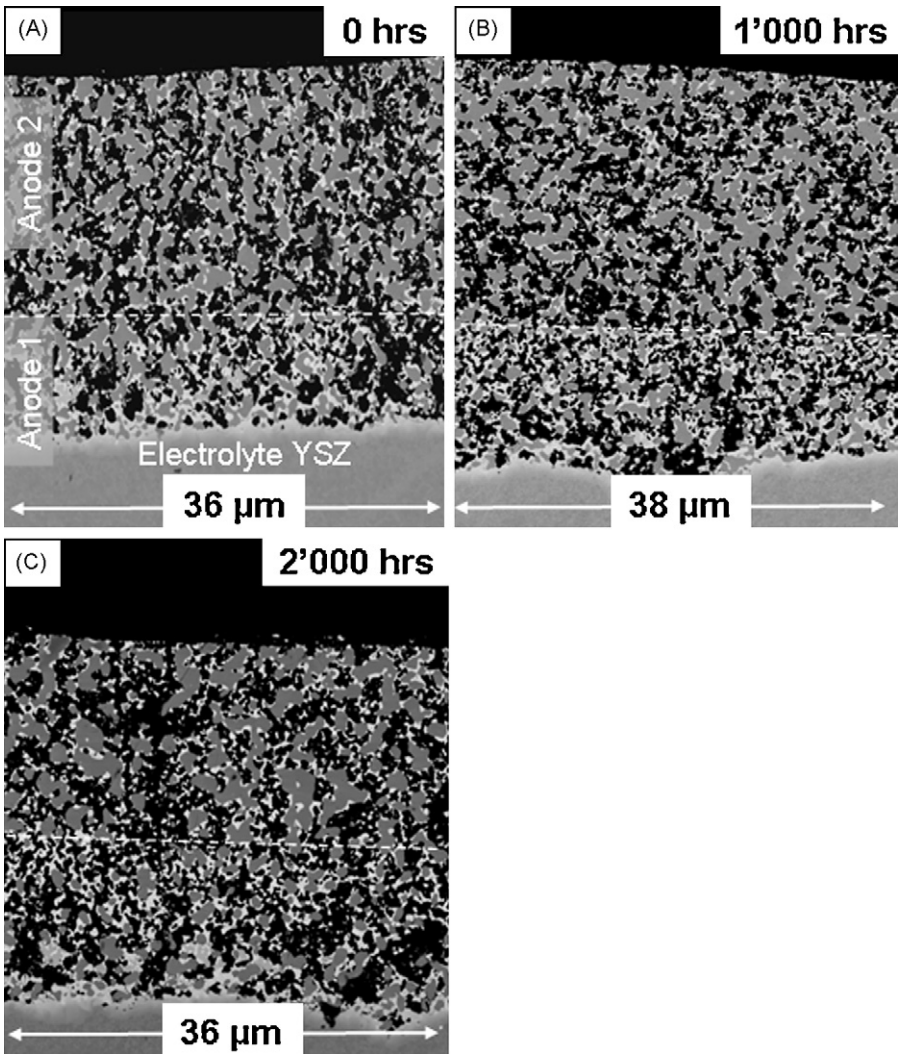

Fig. 7. SEM/BSE images of anode microstructures after exposure to dry forming gas (3% H_2/97% N_2), Nernst-potential: 1.1 V, at 950 °C (experiment A). Ni = grey, CGO = white, pores = black.

With this method the interception lengths from an orthogonal grid or from randomly oriented lines are measured. The resulting chord distribution functions represent the probability of having a specific interception length. However, when considering a bundle of lines with random orientations at the location of a bottle neck, one can observe that very different interception lengths are possible for complex morphologies (Fig. 5, middle). This example illustrates that the interception methods may result in relatively wide size distributions, which are difficult to be interpreted in terms of microstructure–property relationships. In addition, the stereological factor which is used for the correction of sectioning effects in 2D analyses introduces considerable uncertainty for microstructures with complex (non-spherical) particle shapes.

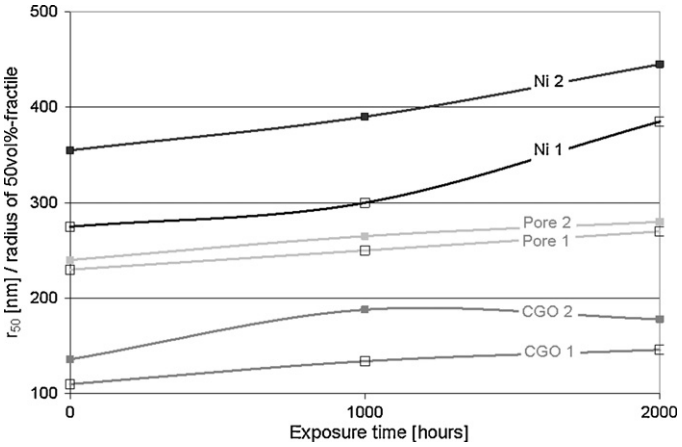

Fig. 8. Change of radius (r_{50}) over time, documenting the grain growth of nickel, CGO and pores in anode layers 1 and 2, after exposure to dry forming gas at 950 °C. (The lines represent the trend of evolution.)

The third method (Fig. 5, bottom) is called continuous PSD_C [27] because it is suitable to characterize continuously percolating phases. It is based on an algorithm which measures the area (2D) or volume (3D) that can be covered with a circle or sphere of a given radius (r_{xyz}). The continuous PSD_C is then obtained by incrementally decreasing the radius and thereby filling increasingly larger area (or volume). By decreasing the radius more constricted areas such as bottle necks and narrow corners can be intruded. This algorithm can thus also be interpreted as a simulation of a liquid intrusion with a poorly wetting fluid such as mercury [38,39].

Compared to the first two PSD techniques, the continuous PSD_C has several important advantages. First of all the continuous PSD_C can be applied to continuously percolating phases without facing the difficulty of object recognition (e.g. by means of splitting). Fur-

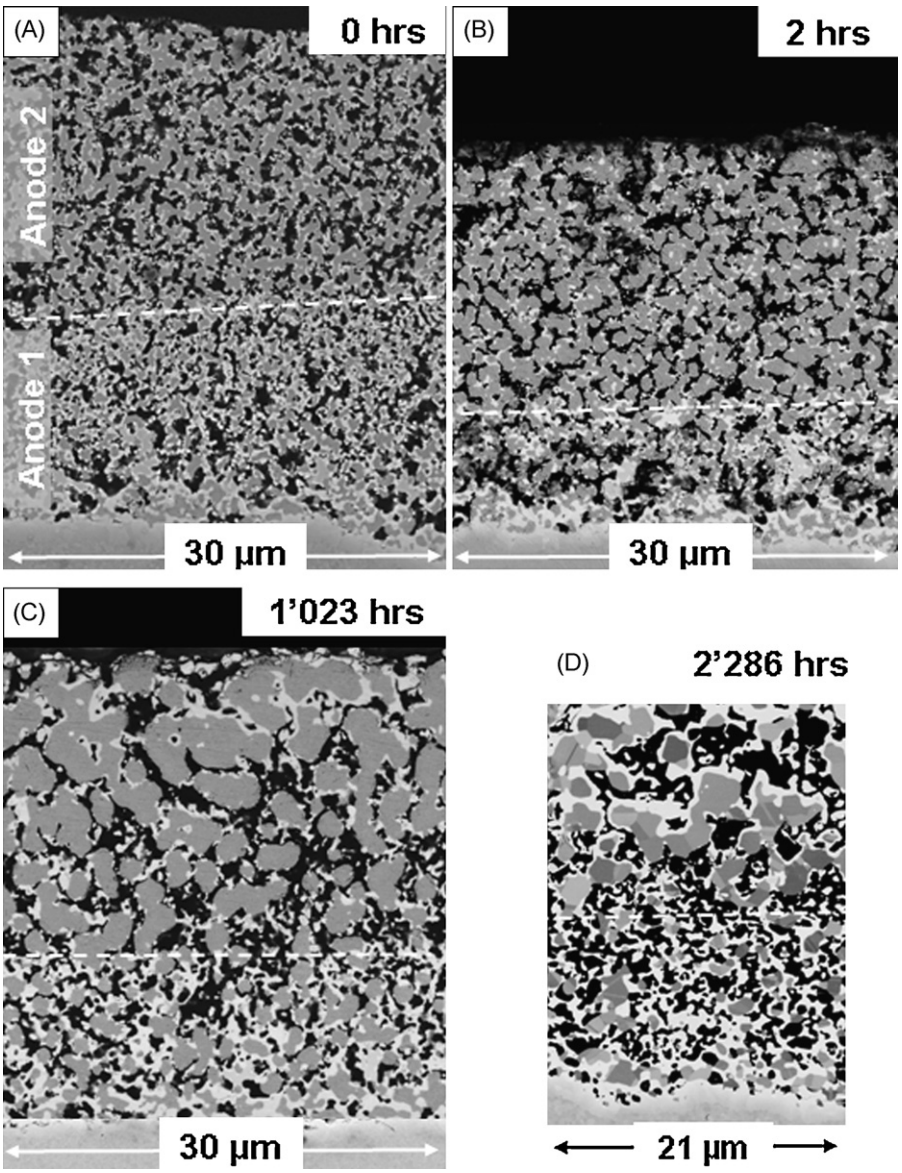

Fig. 9. SEM/BSE images of anode microstructures exposed to a humid gas (Nernst-potential: 0.87 V) at 950 °C. Ni = grey, CGO = white, pores = black. After only 2 h the grain size of Ni is considerably increased. The maximum particle size of Ni has been reached after 1023 h. At longer exposure times (up to 2286 h) no further grain growth of nickel is observed. However during this period the Ni volume fraction is decreasing whereas the volume and particle size of CGO are increasing. (Note that D represents a cross-section from FIB-SEM, because mechanical polishing of this sample resulted in preparation artifacts, as described earlier.)

thermore, it was demonstrated that the continuous PSD_C from 2D images give very similar results as those from 3D tomographic data [40] without application of complicated (and uncertain) stereological correction procedures. Finally, compared to the chord length and intercept methods, the continuous PSD_C does not represent a probability of interception lengths. For each point in the image the continuous PSD_C represents a well defined size measurement. For the characterization of microstructural degradation in SOFC anodes we have therefore decided to use the continuous PSD_C as we believe it is the most suitable, reproducible and reliable PSD technique. More detailed explanations of continuous PSD_C are presented elsewhere [27].

4. Results

4.1. Reproducibility of PSD-measurements

The following section is focusing on the reproducibility of our methodology for quantitative microstructure analysis. For this purpose continuous PSD_C measurements are applied to four different samples of the same anode material. All SEM images were taken at 15 nm pixel resolution with a constant image width of 30 μm. As shown in Fig. 6, for all three phases (nickel, CGO and pores) the four PSD curves are close to each other. The standard deviations of the r_{50} radii are 4.4 nm for CGO, 10.7 nm for nickel and 15.4 nm for the pores. For the measured volume fractions the standard deviations are $\leq$2% for all three phases.

It is important to note that the four samples were screen printed semi-automatically and sintered in different batches. It can thus be expected that the microstructures of the four samples are not perfectly identical due to some variations of the sample production. In addition also the sample preparation may have an effect on the results. Especially the small particles in the sub-μm range tend to be removed from the surface of the sample by mechanical polishing. The measured standard deviations thus represent a maximum estimation for the methodological uncertainty which includes an unknown microstructural variability among the four samples which is not related to the PSD methodology. Similar vari-

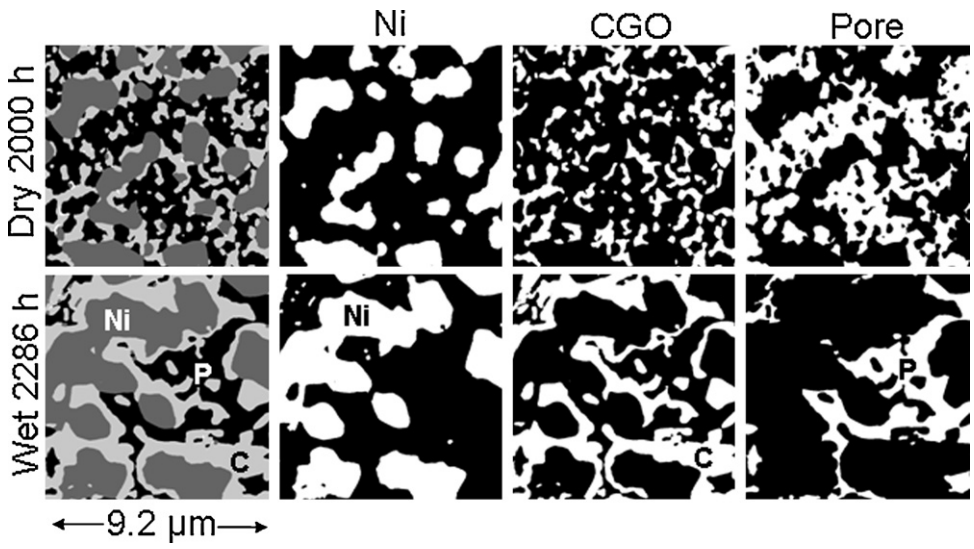

Fig. 10. Comparison of microstructures in anode layer 2 after long time exposure from experiment A (top row) and experiment B (bottom row). Note the difference in the wetting behaviour of CGO on the surface of nickel (dry vs. humid).

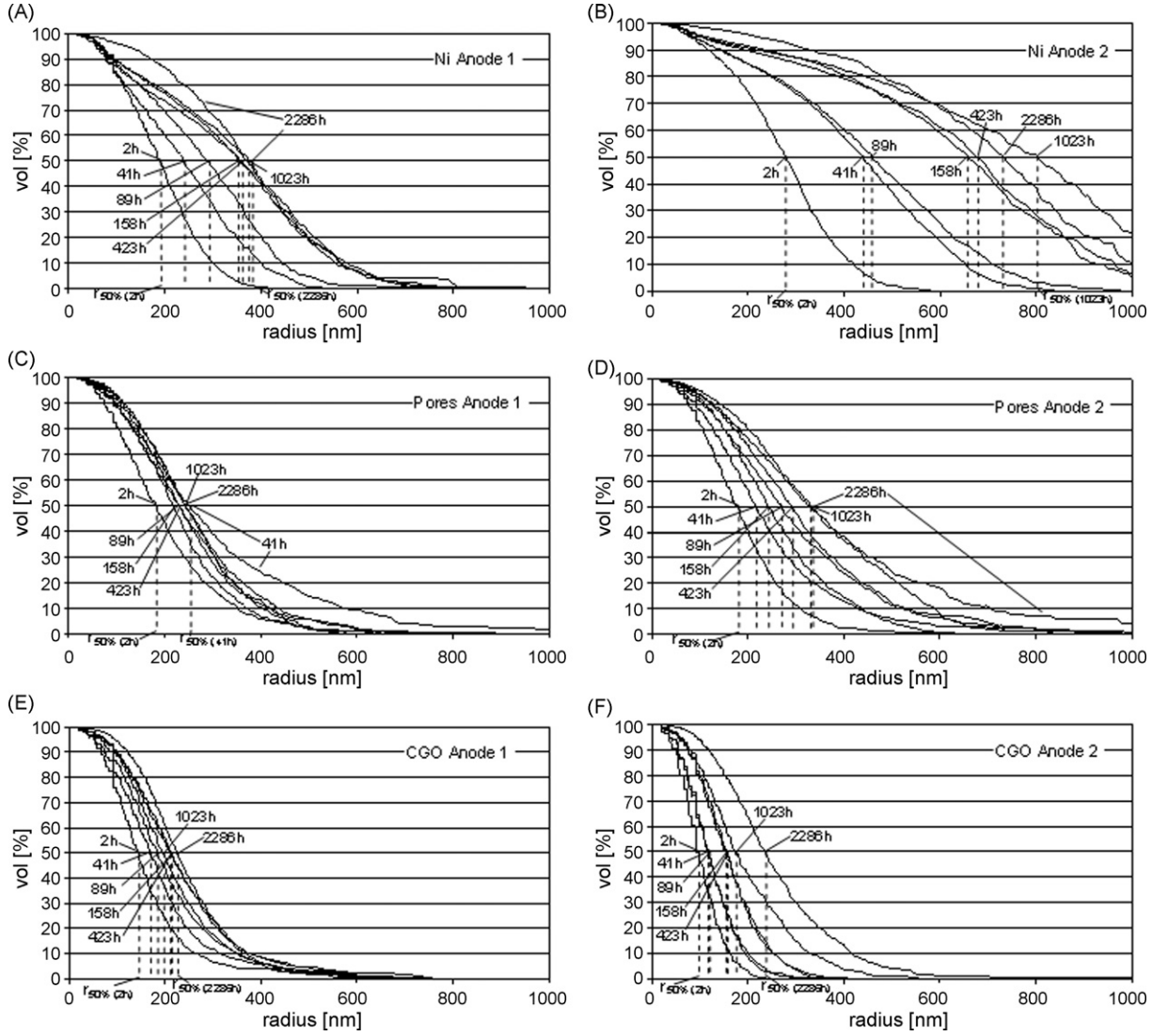

Fig. 11. Continuous phase size distributions (PSD_C) for nickel (top), pores (middle) and CGO (bottom) in experiment B. The anodes were exposed for up to 2286 h to a humid gas at 950 °C. The coarsening of nickel is faster during the first 200 h and decreases at longer exposure times (A and B). Note the different shape of the PSD curve for Ni at 2286 h, related to a decrease of small particles (<300 nm). Overall, the coarsening of pores (C and D) and CGO (E and F) is less pronounced. For all three phases the microstructural changes in anode layer 2 (right) are larger than in anode layer 1 (left). The time dependent changes of the radii at 50 vol.% (r_{50}) are plotted in Fig. 12.

ations also have to be expected among the samples that are used in the degradation experiments. In theory, the method is thus stable and sensitive enough to describe small differences of grain size in the range of 20–30 nm. This method is used subsequently to characterize quantitatively the grain growth associated with microstructural degradation in dry and humid environments.

4.2. Experiment A: microstructural degradation in dry forming gas at 950 °C

The microstructures of anodes that were exposed in a dry forming gas at 950 °C for 0, 1000 and 2000 h are illustrated in Fig. 7. These images qualitatively document that microstructural changes in dry environment are moderate to low. Fig. 8 shows the particle radii (r_{50}) corresponding to the 50 vol.% fractile which are extracted from the continuous phase size distributions. Over the entire period of 2000 h the average nickel radii increase from 280 to 380 nm (anode 1) and from 360 to 450 nm (anode 2). The corresponding growth rates for nickel during the first 1000 h are relatively slow (i.e. 0.91%/100 h in anode 1 and 0.98%/100 h in anode 2). Between 1000 and 2000 h the growth rates are higher (i.e. 2.8%/100 h in anode 1 and 1.4%/100 h in anode 2). These measurements thus indicate that the nickel coarsening in the dry environment is accelerating with time. In contrast the growth rates of the pores and CGO are stable over the entire period of exposure (0.5–0.8%/100 h). For CGO in anode 2 they even tend to decrease with time. Nickel grain growth is thus the dominant feature of microstructural degradation in the dry environment.

4.3. Experiment B: microstructural degradation in humid gas at 950 °C

As illustrated qualitatively in Fig. 9 microstructural degradation in the presence of water vapour is much stronger and faster than in the dry environment (Fig. 7). In the humid environment the grain size of nickel has significantly increased after only 2 h (Fig. 9B). However, at longer exposure time (i.e. between 1023 h (Fig. 9C) and 2286 h (Fig. 9D)) the particle size of nickel remains stable.

Already on a qualitative level it becomes obvious that very different microstructures result from long time exposure (2000 h) in dry and in humid environments. Thereby the grain growth of nickel is not necessarily the most prominent feature. As shown in the binary images at higher magnification (Fig. 10) the microstructural differences after dry and wet exposure are also significant for the CGO and for the pore structures. In experiment A (dry) CGO maintains its granular texture (Fig. 10, top) similar to the initial microstructure. In contrast in experiment B (humid) CGO forms a continuous layer on the surface of nickel (Fig. 10, bottom). The improved wetting of CGO in the humid environment thus leads to a shielding of the nickel grains which may hinder further grain growth of nickel at long time exposure.

The continuous phase size distributions (PSD_C) in the anodes that were exposed to a humid gas are shown in Fig. 11. For all three phases the microstructural changes are larger in anode layer 2. Nickel grain growth is very fast during the first 158 h and after 1023 h no significant Ni coarsening was seen (Fig. 11A and B). However, the shapes of the PSD curves at 2286 h are markedly different compared to the other PSD curves of nickel. It indicates a lower number of small particles in the range 50–300 nm. CGO is expected to be much more stable than Ni and indeed only relatively small changes of the PSD curves are observed for CGO. However, in contrast to the Ni and pore phases, CGO in anode layer 2 (Fig. 11F) is still growing at long exposure times (>1000 h). This behaviour may be related to the observed formation of a continuous CGO layer on the nickel surface (Fig. 10, bottom).

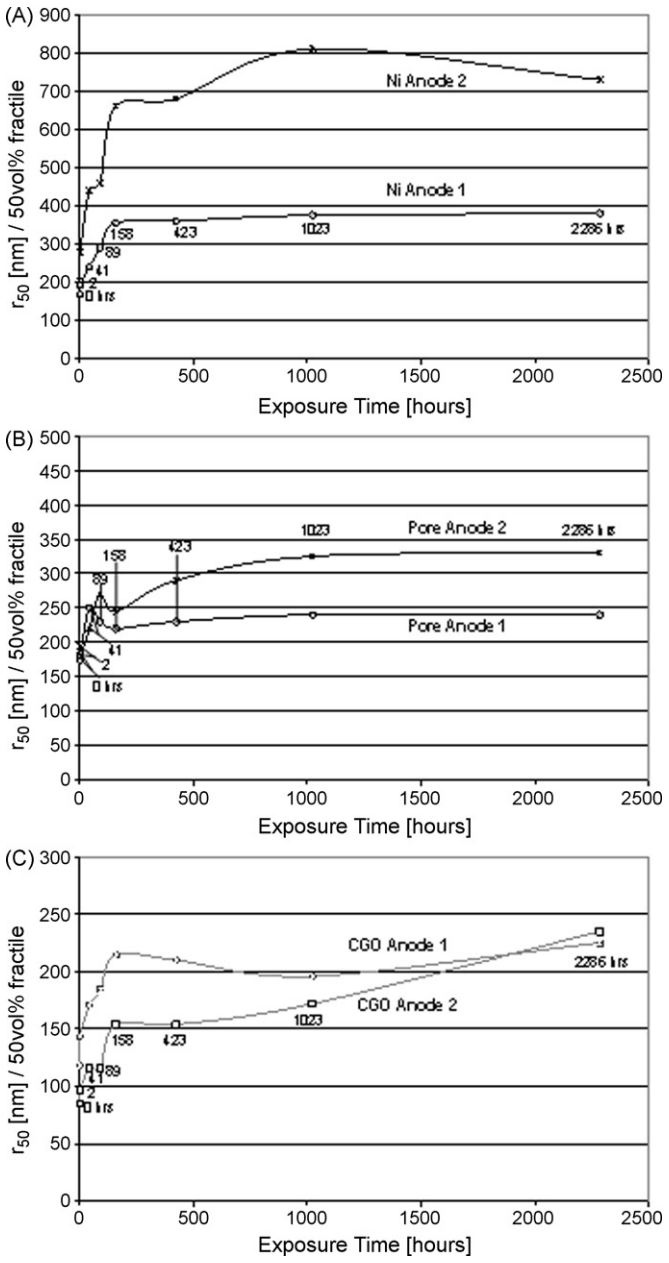

Fig. 12. Evolution of particle and pore radii (r_{50}) over time in experiment B. The anode samples were exposed to a humid gas environment at 950 °C. Top: nickel, Middle: pore, Bottom: CGO.

The particle and pore radii at 50 vol.% are extracted from the corresponding PSD curves in Fig. 11 and plotted over time in Fig. 12. The evolution of these radii (r_{50}) indicates that the degradation rates are not constant (Fig. 12). For all three phases faster grain growth is observed during the initial period (0–158 h). At longer exposure times (>1000 h) an apparent plateau with a maximum particle size is reached for Ni and for the pores. In contrast the CGO particles of anode layer 2 are still growing after 1000 h.

It has to be mentioned that the single data points in Fig. 12 do not provide perfectly smooth growth curves. As shown earlier in Fig. 6 the standard deviations for the measurement of PSDs and r_{50} radii from our reference samples are approximately 10 nm. However, the fluctuations in our measurements in experiment B (Fig. 12) are larger than 10 nm (approximately 50 nm) which indicates some true microstructural variations among the samples. It was observed that sample preparation by mechanical grinding and polishing may

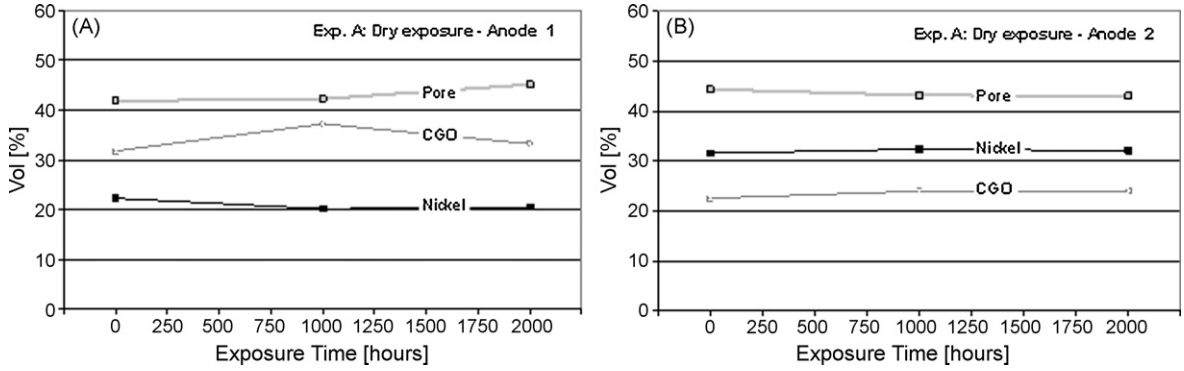

Fig. 13. Volume fractions of nickel, CGO and pore phases in samples exposed to dry gas environment (experiment A).

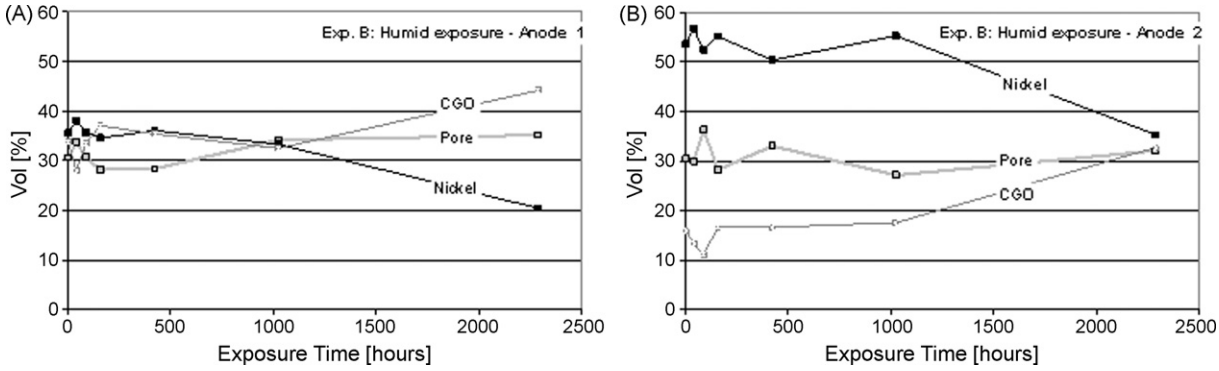

Fig. 14. Volume fractions of nickel, CGO and pore phases in samples exposed to humid gas environment (experiment B).

lead to artifacts whereby CGO tends to burst from the sample surface. The observed fluctuations are thus attributed to such problems with sample preparation.

4.4. Changes of volume fractions during experiments A and B

Simple Ostwald ripening usually leads to a local microstructural reorganization which does not include any changes of the bulk composition. In contrast, volatilization and re-precipitation can lead to locally different compositions. In this context, it has to be mentioned that the samples for experiments A and B do not have the same initial compositions because the anode production was made with two different batches of paste mixtures.

The volume fractions of the samples in experiment A (Fig. 13) are measured from the images in Fig. 7. The measured compositional changes are in the range of the methodological standard deviation (2%), which was obtained from reference samples (Fig. 6). The anode composition thus remains stable during exposure in a dry environment. In contrast the compositions of samples from experiment B (humid conditions) show a more complicated picture (Fig. 14). The most prominent feature is the decrease of Ni during the period of 1023–2286 h. A removal of nickel from the microstructure at constant electrode volume would induce an increase of the porosity. However, the pore volume fraction remains nearly constant whereas the volume decrease of Ni is compensated by an increase of CGO. This could be explained with volumetric shrinkage that is contemporaneous with the removal of nickel. The data points in Fig. 14 also indicate variations during the earlier stages of the experiment in the range of ±5%. Thus, in a similar way as previously discussed for the fluctuations of r_{50} radii in Fig. 12, the variations of volume fractions in Fig. 14 are larger than the methodical standard deviations (2%). Apparently there are microstructural variations between the different samples which could have formed during sample preparation. Nevertheless, the extent of the Ni vol-

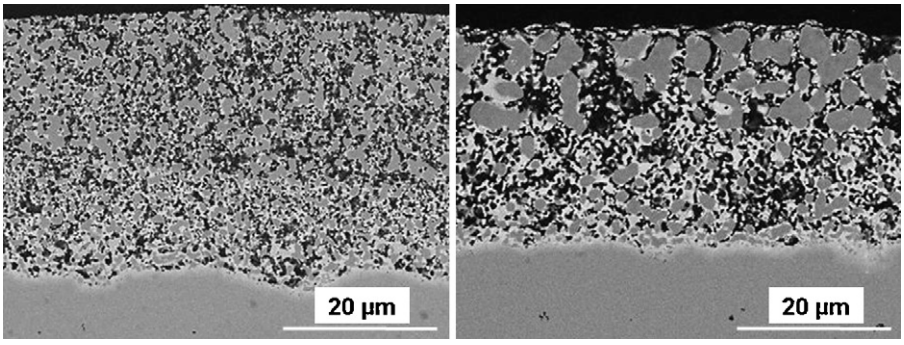

Fig. 15. SEM images of identical anode material, documenting the influence of different flow rates on the coarsening of nickel. Both samples were exposed for 200 h at 950 °C to a gas mixture with 60% H_2O (OCV: 870 mV). For the left sample the flow rate of $H_2O_{(g)}$ was only 0.8 ml h^{-1} whereas for the right sample the flow rate of $H_2O_{(g)}$ was 6 ml h^{-1}.

ume reduction at long exposure times (2286 h) is larger than the fluctuations during earlier periods in Fig. 14, which indicates that the depletion of nickel is a significant feature of the long time exposure in humid gas.

4.5. Experiment C: microstructural degradation under different H_2O flow rates at 950 °C

To further investigate the influence of the water vapour on the microstructural degradation, the same anode samples were exposed to different H_2/H_2O flows at 950 °C (see Table 1). The Nernst-potential was kept constant at 0.87 V, by changing the H_2 and H_2O flow proportionally. In other words, the ratio of water vapour and H_2 was constant. Since the H_2/H_2O flow was diluted with 200 ml min^{-1} N_2 the differences in the total mass flow are considered to play a minor role (see Table 1).

Fig. 15 shows two samples of the same initial Ni/CGO composition. The sample on the left was exposed to relatively low H_2/H_2O flow rates (0.8 ml h^{-1} H_2O and 6 ml min^{-1} H_2). The sample on the right was exposed to much higher H_2/H_2O flow rates (6 ml h^{-1} H_2O and 30 ml min^{-1} H_2). The comparison in Fig. 17 clearly documents that grain growth of nickel is strongly correlated with the flow rates of H_2/H_2O.

5. Discussion

5.1. Methodological and experimental reproducibility

Before interpreting the data from experiments A and B in the view of possible degradation mechanisms and before discussing the influence of different environmental and compositional parameters it is necessary to re-evaluate the methodological and experimental uncertainties. Each step of our methodology for microstructure analysis was evaluated critically in this study:

(A) During sample preparation with mechanical grinding and polishing, CGO tends to burst from the sample surface which may result in artificially high porosities. Minor fluctuations in the growth curves of nickel, CGO and the pores may thus be the result from these problems with the sample preparation. For delicate samples (e.g. experiment B at 2286 h) these preparation artifacts can be avoided by using the focused ion beam (FIB) technique which allows production of perfectly flat cross-sections.

(B) Image acquisition with a solid state BSE detector requires a minimum accelerating voltage of 5 kV which limits the physical resolution and leads to apparently 'diffuse' transition zones at the interface between the neighbouring phases. In our fine grained anode material these transition zones may represent up to 15% of the total image area.

(C) For accurate identification of the grain boundaries, the pixels from the transition zones are assigned to the neighbouring phases with a special segmentation procedure that is based on an asymmetric region growing process. In this way the draw back of a limited resolution at ≥5 kV can be largely corrected.

(D) For precise and reproducible analysis imaging resolution and window size must be chosen according to the size distribution and to the homogeneity of the sample. For the initial microstructure a parametric study shows that a pixel resolution of max. 35 nm and a window size of min. 400 μm^2 results in precise and reproducible PSD measurements. During the degradation experiments grain size and microstructural heterogeneity increase and therefore a larger image window is necessary for reproducible analysis. Consequently, in this study each PSD measurement is based on a window size of at least 600 μm^2.

(E) The continuous PSD_C method which is used in this study has several advantages compared to the discrete and intercept methods. In previous studies it was shown that the continuous PSD_C provides nearly identical results from 2D images as from 3D tomographs [27,40]. Thereby, neither stereological correction nor sophisticated object recognition are necessary. We have therefore decided to use the continuous PSD_C as we believe that it is the most suitable method for the description of grain growth in the percolating networks of nickel, CGO and pores.

The reproducibility of the refined method for microstructure analysis was evaluated based on the investigation of four reference samples with the same anode composition. The analyses of reference samples provide maximum estimations for the standard deviations of the r_{50} radii, which are 10 nm for Ni, 16 nm for Pores, 5 nm for CGO and less than 2% for the measurement of volume fractions (see Fig. 6). The evolution of the r_{50} radii during exposure in a wet environment shows fluctuations which are larger than these methodological uncertainties (Fig. 12). In a similar way the compositional variations (i.e. the measured volume fractions of each phase) in experiment B (Fig. 14) are larger than the methodological standard deviation of 2%. The reason for that is unclear and might be related to the mechanical polishing of the sample. Nevertheless, the broad evolution of the measured grain growth in both experiments and the observed decrease of nickel volume at long exposure time in experiment B are much larger than the mentioned fluctuations. These features are thus considered as being relevant and reproducible phenomena of the microstructural degradation which are discussed in the following sections.

5.2. Growth rates of nickel – comparison with literature

When comparing the microstructural data from different authors it is usually only discussed in what way the experimental and compositional parameters (e.g. different temperature, gas flow, gas composition, anode composition and microstructure) may affect the observed degradation patterns. However, very different results must be expected when different PSD techniques are applied because of the contrasting geometrical models that are inherent to each of these techniques. Thus, even in the case where the methodological precision and accuracy are excellent, the comparability of results from different authors may be limited. Therefore in the following comparison of data sets from different authors only clear trends and marked patterns will be considered as significant features related to the anode degradation.

Growth rates from literature data (see Fig. 2) and from our own experiments are summarized in Fig. 16. In all the studies from literature (see Fig. 2) the experimental conditions are comparable to our experiment B with humid gas composition. The data from all these studies reveals a common pattern which is characterized by faster growth rates during the initial period and a significant decrease of the growth rates at longer exposure time (>1000 h). At long exposure time in anode 2 even a 'negative growth' is observed (experiment B, humid) which may be related to the contemporaneous decrease of the nickel volume between 1023 and 2268 h (see Fig. 14). This decrease of growth rates may indicate a change of the coarsening mechanism over time under humid conditions. In this context, the observed 'negative growth' is considered as a strong indication for the volatilization of nickel via gas phase which was also reported by Hagen et al. [18].

Overall, the initial coarsening in experiment B (up to 140%/100 h) is much faster than the growth rates extracted from literature data. One possible reason for the apparently faster growth

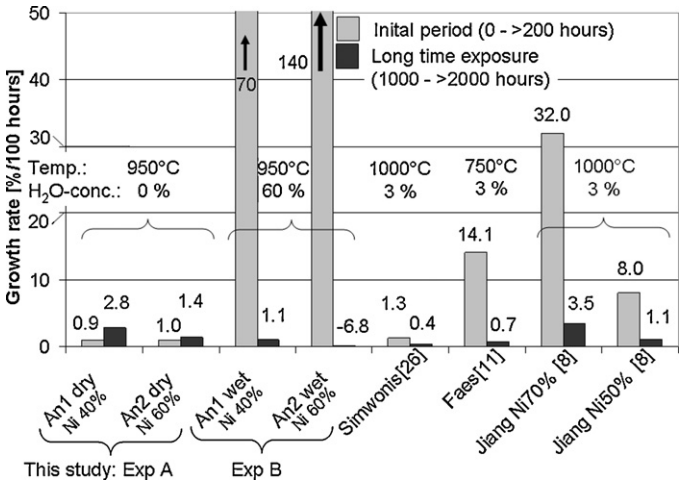

Fig. 16. Growth rates of nickel during the initial period (<200 h, bright grey) and during long time exposure (>1000 h, dark grey). Growth rates from experiment A (dry gas), experiment B (humid gas) and from literature are compared with each other. The literature values are extracted from the growth curves in Fig. 2.

rates in experiment B may be the higher water content (60%) in combination with a relatively fast gas flow (6 ml h^{-1}). The effects of gas flow and water concentrations on the degradation rate are discussed below (see Fig. 15).

The comparison of growth rates in experiments A and B also document a very different coarsening behaviour of dry and humid environments. Thereby the coarsening in the dry environment is considerably slower during the initial period (only 1%/100 h) and in contrast to the humid conditions the growth rates increase slightly (1.4% and 2.8%) at longer exposure time in the dry experiment. Hence, there is a marked difference between dry and humid conditions with respect to the degradation kinetics and its evolution over time. This difference may be due to the different chemical reactions associated with the presence of water, whereby formation and transport of nickel hydroxides apparently plays a major role in the coarsening history. In addition there are also feedback-effects of microstructural changes (which are different in dry and humid environments) on the coarsening itself. For example in humid environment there are indications for a change of the nickel volume fraction due to volatilization which is also associated with a relative enrichment of CGO compared to nickel. As a feedback the higher CGO to nickel ratio leads to a higher coverage of nickel and formation of CGO layers, which then protect the nickel grains from further coarsening. Such feedback effects are not expected in the dry environment, where the nickel volume fraction remains unchanged over the entire period of investigation.

5.3. Summary of observed degradation phenomena

The degradation experiments in dry and humid gas reveal a puzzling picture with numerous microstructural degradation phenomena that are not restricted to Ni coarsening alone. The quantitative results as well as the most important qualitative observations are illustrated schematically in Fig. 17. The labels A to F in the subsequent discussion refer to Fig. 17:

(A) One of the most prominent features of anode degradation in a humid gas is the uneven evolution of the growth rates over time with a very fast nickel coarsening during the initial phase and stagnation of grain growth at long exposure time (Fig. 12). It was shown in the literature that the growth curves of nickel characterized by fast initial coarsening followed by formation of an apparent plateau with a maximum particle size can be modelled either with a so-called 'charge capacitor model' [11] or with a so-called two-particle model [21]. Similar trends were also observed in our experiments.

(B) The degradation in a dry environment is characterized by much lower growth rates during the initial period and by a slight increase of the growth rates at longer degradation time (Fig. 8).

(C) The effect of anode composition on degradation kinetics is characterized by the systematic differences between anode layer 1 (60 vol.% CGO, 40 vol.% Ni) and anode layer 2 (40 vol.% CGO, 60 vol.% Ni). In all experiments microstructural degradation of anode layer 1 is slower than in anode layer 2. The reduced grain growth in anode 1 can be attributed to the stabilizing effect of a higher ceramic content (compare Fig. 11A, Fig. 11B and Fig. 14). These findings are also compatible with the observation of faster growth rates for anodes with a higher ratio of Ni/YSZ [8].

(D) A further observation in the humid environment is the decrease of the nickel content at long exposure time (mainly in anode layer 2). In analogy to other studies [18,20] this compositional change may be an evidence for the volatilization of nickel species via the gas phase. In experiment B, the volumetric loss of nickel is compensated by a relative increase of CGO (Fig. 14).

(E) During long time exposure in humid gas the microstructural degradation is not just related to changes in the nickel diameter but also to textural changes of CGO and porosity. In particular, the formation of a continuous CGO layer surrounding the nickel grains was observed (Fig. 10). The CGO, which covers the nickel grains to a large degree, may act as a protective layer which decreases the Ni-coarsening. In contrast, in the dry environment the CGO phase maintains its granular texture which is very similar to the initial microstructure before degradation. The different morphologies of CGO in dry and humid environments could be attributed to different effects. The mentioned reduction of the nickel volume fraction due to volatilization of nickel hydroxides leads to an increase of CGO relative to nickel (D). Purely volumetric changes could thus be the reason for a higher coverage of the nickel surface by the ceramic phase. In addition the formation of surface hydroxide species may lead to a change of the wetting behaviour between CGO and nickel. The presence or absence of surface hydroxide species may thus be an additional reason for different wetting behaviours in dry and humid conditions. At this stage it has to be mentioned that the chemical details of the surface wetting mechanism have not been investigated in the present study.

(F) The PSD may have a strong effect on growth rates as discussed in the introduction for the 'two particle model' [21]. This effect is related to the increased reactivity of small particles in the nano- to sub-μm range. During degradation in a humid environment the PSD curves are not only shifted towards larger particle sizes but also the shapes of the PSD curves are changed at long exposure times. Thereby the changing shape of PSD curves for nickel indicates a marked reduction of the smallest particle size class (<300 nm) at long exposure time (Fig. 11). Reduction of small nickel particles may be contemporaneous with the observed volatilization of nickel and the formation of continuous CGO layers on the surface of large nickel particles. The change of PSD over time appears to be linked with a change of the growth rates.

5.4. Effect of environmental and compositional parameters on degradation kinetics

The above summarized pattern of degradation phenomena give clear evidence in what way different parameters influence the kinetics of microstructural changes. In addition they also give an indication under which conditions the dif-

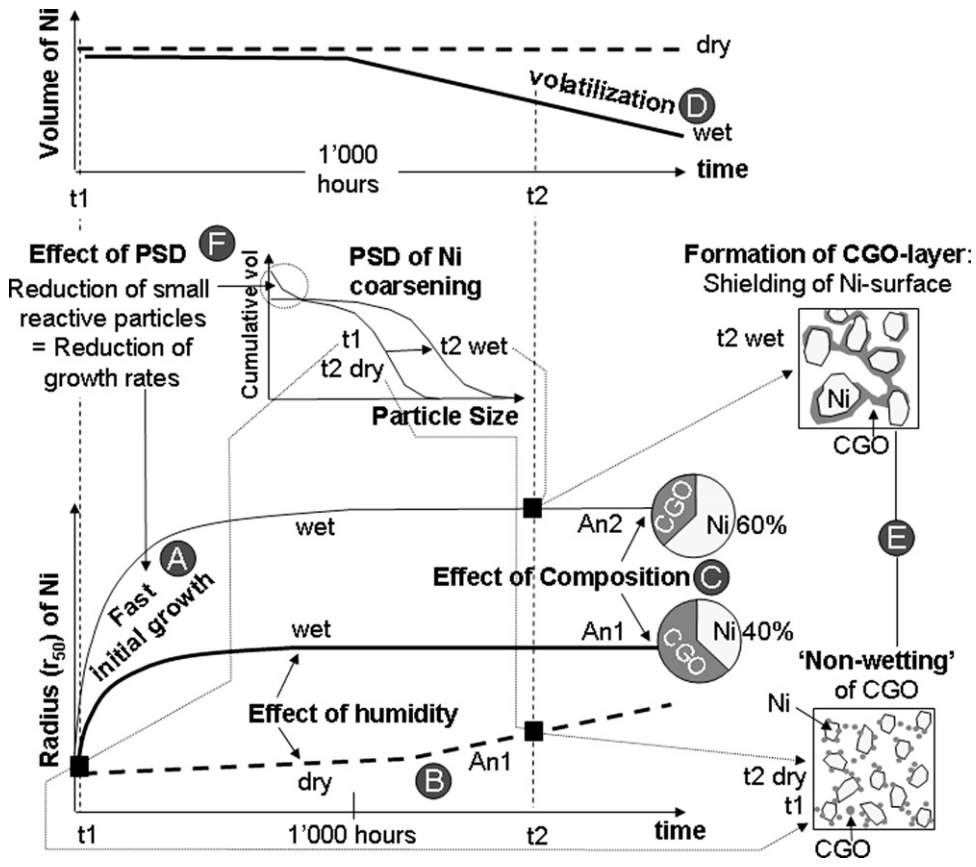

Fig. 17. Summary of degradation phenomena (quantitative and qualitative) which are observed in experiments A and B.

ferent degradation mechanisms become more prominent or not.

5.4.1. Enhanced growth kinetics in humid conditions (see Fig. 17A and B)

As discussed in the introduction the kinetics of the different degradation mechanisms (e.g. volatilization of nickel hydroxides, Ostwald ripening, surface diffusion) is strongly enhanced by the presence of H_2O in the gas phase. The thermodynamic data of the system Ni, H_2 and O_2 (Fig. 2) shows that the vapour pressure of $Ni(OH)_2$ is six orders of magnitude higher than the vapour pressure of pure Ni [20]. Therefore, small concentrations of water vapour (1–2%) in the gas phase will increase the mobility of volatile nickel species considerably. The experimental finding of accelerated coarsening in a humid environment is most likely linked to the formation of $Ni(OH)_2$ as seen from the thermodynamic data (Fig. 1). Nevertheless, the different evolutions of growth rates over time in dry (increasing growth rates) and in humid environments (decreasing growth rates) cannot be explained simply by the different thermodynamic properties.

5.4.2. Decreasing growth rates due to Ostwald ripening and shielding of nickel by CGO (see Fig. 17A, E and F)

The change of the degradation kinetics from very fast initial coarsening to nearly zero grain growth at long exposure times may have different reasons. First of all, the experimental trend of Ni coarsening fits with the type of Ostwald ripening which is driven by the different curvatures of neighbouring particles as described with the 'two particle model' [21]. Due to the ongoing Ostwald ripening the smaller particles disappear and hence the driving force for grain growth is reduced at longer exposure time. Indeed when comparing the shapes of PSD curves from 1023 to 2068 h (see Fig. 11A and B) a marked reduction in the amount of small particles (<300 nm) is observed at increasing time. Furthermore, decreasing growth rates may also be caused by the formation of a continuous CGO layer (see Fig. 10) which leads to a protective shielding of the nickel grains. The CGO layer may prevent further grain growth at longer exposure times (>1000 h). As a consequence the reaction constant of Ostwald ripening may change over time due to the shielding effect of the CGO-layer.

5.4.3. Volatilization and shielding of nickel at long exposure time in humid conditions (see Fig. 17D and E)

Between 1000 and 2300 h the nickel content in anode 2 is significantly reduced. The decrease of nickel contents is considered as evidence for nickel volatilization at long exposure times which is related to the high partial pressure of $Ni(OH)_2$ in the humid gas of experiment B (60% H_2O). The reduction of the nickel content in combination with an apparent shrinkage (i.e. pore volume remains stable) may lead to a relative increase of CGO. In this way the ratio of CGO to nickel is increased. This may favour the formation of a continuous surface layer of CGO on nickel. Note: In Fig. 12 it was shown that the CGO particle size is not stable over time in the humidified H_2/N_2 gas atmosphere. The shielding of nickel grains by CGO may therefore be initiated by the evaporation of nickel. On the other hand the shielding also protects the nickel grains from further volatilization so that stabilization may be expected after microstructural reorganization at around 2000 h.

5.4.4. Apparent acceleration of nickel coarsening at long exposure time in dry gas (see Fig. 17B)

In accordance with the thermodynamic data from literature the growth rates of nickel are very slow in the absence of water vapour. However, in the dry environment the growth rates do not decrease

at long exposure time, as it would be expected in the case of Ostwald ripening. Under dry conditions the ripening may be too slow so that the deceleration effect due to reduction of small particles cannot yet be observed after 2000 h. However, the results from experiment A even indicate acceleration of nickel growth with time. A possible reason for the increasing growth rates may be related to the joining of neighbouring particles. This apparent coalescence only takes place when the increase of particle size is larger than the initial separation distance between the particles. In the moment when neighbouring particles merge together this leads to apparently high growth rates. In dry conditions this effect of particle coalescence may take place only after more than 1000 h whereas in humid conditions it occurs already during the initial period.

5.4.5. Effect of gas flow rate (see Fig. 15)

In order to understand the complex dynamics of the degradation processes in SOFC anodes also the effect of different gas flow rates at the same H_2O concentration were investigated in experiment C (see Fig. 15). Microstructures of anodes that were exposed to different gas flows at 950 °C showed a significantly slower Ni-coarsening when the flow rate of H_2/H_2O was reduced. The experiment C thus indicates that the total amount of water vapour may have a significant impact on the degree of Ni-coarsening. One explanation may be that the equilibrium between adsorbed H_2O on the Ni-surface is not reached for small H_2/H_2O flows, since in this case only a relatively small number of H_2O molecules can adsorb on the relatively large Ni-surface. The transport of nickel may therefore not only depend on thermodynamic equilibrium conditions but also on dynamic aspects such as the H_2/H_2O flow rates and on the associated total flux integrated over time. The flow of H_2/H_2O per cell area and most likely also the flow velocity may therefore be important parameters when investigating Ni-coarsening. In this context it is important to note that the water vapour in a cell under operation is depending on the current density. For example in our test stacks which consists of five cells the amount of water vapour that is produced at 250 mA cm^{-2} is 6 g h^{-1}. For the comparison with the degradation experiments the gas flow has to be normalized by the surface area of the anode: In the test stack 6 g h^{-1} are flowing over 100 cm^2 whereas in the degradation experiment B the same amount of water (6 g h^{-1}) is flowing over a surface area which is 400 times smaller (0.25 cm^2). Compared to the real conditions in the test stack the gas flux of water vapour is thus considerably higher in our experiment B, which can be interpreted as an accelerated degradation test.

6. Conclusions

For the present study we have optimized the methodology for quantification of microstructural degradation. Special emphasize is led on a reliable procedure for segmentation and feature recognition. In addition a novel algorithm for continuous PSD measurement [27] is used which is capable to describe the size distributions of continuously networked structures based on 2D images. This method is used to quantify the grain growth of nickel in porous SOFC anodes under dry and humid conditions. The biggest difference in the evolution of degradation kinetics over time is observed between dry and humid conditions. In the presence of water vapour diffusion, volatilization and the associated coarsening are strongly increased. During the initial period (0–200 h) grain growth in the humid environment is faster (up to 140% per 100 h). At long exposure times the formation of a continuous CGO layer seems to prevent further grain growth. In contrast, in the dry environment growth rates are stable over a long time span and they even tend to increase at longer exposure from ≤1% to 1.5–3% per 100 h. However the degradation kinetics is not only controlled by the humidity (i.e. by the concentration of $H_2O_{(g)}$). Also the gas flow rate has a very strong influence on the degradation rates. Furthermore compositional effects (ratio between nickel and CGO) and initial particle size also affect the resulting degradation pattern.

Microstructural degradation of nickel cermet anodes thus includes many different processes, parameters and phenomena. Thereby the grain growth of nickel certainly represents an important feature. However, many other microstructural changes were observed. Based on the experiments presented in this study, the kinetics of nickel grain growth cannot be explained solely by a simple Ostwald ripening mechanism. The grain growth of nickel may be influenced by other (contemporaneous) degradation processes such as the evaporation of nickel and the formation of continuous ceramic layers on the surface of the nickel grains at longer exposure times. There is thus a complex interplay between nickel grain growth (e.g. by surface diffusion), volatilization and microstructural reorganization which includes the geometrical distribution of the other phases (CGO and pores).

In the present study the emphasis is led on the quantification of grain growth in combination with qualitative observations. However, there are other parameters such as the triple phase boundary length (TPB_L) and the catalytic surface area of nickel which are considered to have a more direct influence on the electrochemical performance [11]. At this stage the link between TPB_L and electrochemical degradation is not yet established quantitatively. From the qualitative observations in this study it can be concluded, that the formation of a continuous CGO layer on the nickel grains certainly leads to a reduction of the TPB_L (and of the catalytically active surface area of nickel). In this context it is important to note that the improved methodology for microstructure analysis as presented in this study enables a precise recognition of phases and objects which is the basis also for a reliable quantification of TPB_L and surface area. First results of a quantitative description of TPB_L and its correlation with nickel grain growth are described in separate papers [41] which are based on 3D-analyses by FIB-nanotomography [42].

Acknowledgements

The research presented in this paper was performed within the framework of a Swiss national project (SFOE project No. 102290: SOF-CH) and an ERA-NET project (SFOE project No. 102746: AccelenT). Financial support by the Swiss Federal Office of Energy (SFOE) and by Swisselectric Research is gratefully acknowledged.

References

[1] H. Yokokawa, H. Tu, B. Iwanschitz, A. Mai, Journal of Power Sources 182 (2008) 400–412.
[2] J.-M. Klein, S. Georges, Y. Bultel, Journal of the Electrochemical Society 155 (2008) B333–B339.
[3] K. Haga, S. Adachi, Y. Shiratori, K. Itoh, K. Sasaki, Solid State Ionics 179 (2008) 1427–1431.
[4] B. Iwanschitz, J. Sfeir, A. Mai, M. Schütze, Journal of the Electrochemical Society 157 (2010) B269–B278.
[5] T. Klemenso, M. Mogensen, Journal of the American Ceramic Society 90 (2007) 3582–3588.
[6] D. Sarantaridis, A. Atkinson, Fuel Cells 07 (2007) 246–258.
[7] J.-H. Lee, H. Moon, H.-W. Lee, J. Kim, J.D. Kim, K.-H. Yoon, Solid State Ionics 148 (2002) 15–26.
[8] S.P. Jiang, Journal of Materials Science 38 (2003) 3775–3782.
[9] A. Ioselevich, A.A. Kornyshev, W. Lehnert, Journal of the Electrochemical Society 144 (1997) 3010–3019.
[10] A. Ioselevich, A.A. Kornyshev, W. Lehnert, Solid State Ionics 124 (1999) 221–237.
[11] A. Faes, A. Hessler-Wyser, D. Presvytes, C.G. Vayenas, J. Van Herle, Fuel Cells 6 (2009) 841–851.
[12] A. Bieberle, L.P. Meier, L. Gauckler, Journal of the Electrochemical Society 148 (2001) A646–A656.
[13] W.G. Bessler, J. Warnatz, D.G. Goodwin, Solid State Ionics 177 (2007) 3371–3383.

[14] J.R. Wilson, W. Kobsiriphat, R. Mendoza, H.-Y. Chen, J.M. Hiller, D.J. Miller, K. Thornton, P.W. Voorhees, S.B. Adler, S.A. Barnett, Nature Materials 5 (2006) 541–544.
[15] J. Mizusaki, H. Tagawa, T. Saito, K. Kamitani, T. Yamamury, K. Hirano, S. Whara, T. Takagi, T. Hikita, M. Ippommatsu, S. Nakagawa, K. Hasgimoto, Journal of the Electrochemical Society 141 (1994) 2129–2134.
[16] P. Tanasini, M. Cannarozzo, P. Costamagna, A. Faes, J. Van Herle, A. Hessler-Wyser, C. Comninellis, Fuel Cells 5 (2009) 740–752.
[17] T. Iwata, Journal of the Electrochemical Society 143 (1996) 1521–1525.
[18] A. Hagen, B. Rasmus, P.V. Hendriksen, Y.-L. Liu, S. Ramousse, Journal of the Electrochemical Society 153 (2006) A1165–A1171.
[19] S. Elangovan, A. Khandkar, Int. Symposium Ionic and Mixed Conducting Ceramics, The Electrochemical Society ECS, Arizona, 1991, pp. 122–132.
[20] A. Gubner, H. Landes, J. Metzger, H. Seeg, R. Stübner, 192nd Meeting of the Electrochemical Society, ECS, Paris, 1997, pp. 844–850.
[21] R. Vassen, D. Simwonis, D. Stöver, Journal of Materials Science 36 (2001) 147–151.
[22] W.D. Halstead, Corrosion Science 15 (1975) 603–615.
[23] J. Israelachvili, Intermolecular and Surface Forces, Academic Press, Elsevier, Amsterdam, 1991.
[24] J. Sehested, Catalysis Today 111 (2006) 103–110.
[25] J. Sehested, J.A.P. Gelten, S. Helveg, Applied Catalysis (A) 309 (2006) 237–246.
[26] D. Simwonis, F. Tietz, D. Stöver, Solid State Ionics 132 (2000) 241–251.
[27] B. Münch, L. Holzer, Journal of the American Ceramic Society 91 (2008) 4059–4067.
[28] L.A. Giannuzzi, F.A. Stevie, Micron 30 (1999) 197–204.
[29] L. Holzer, M. Cantoni, in: P. Russell, I. Utke, S. Moshkalev (Eds.), Nanofabrication with Focused Electron and Focused Ion Beam, Oxford University Press, in press.
[30] K. Thydén, Y.L. Liu, J.B. Bilde-Sorensen, Solid State Ionics 178 (2008) 1984–1989.
[31] I. Cousin, P. Levitz, A. Bruand, European Journal of Soil Science 47 (1996) 439–452.
[32] P. Levitz, Advances in Colloid and Interface Science 76–77 (1998) 71–106.
[33] K.N. Grew, Y.S. Chu, J. Yi, A.A. Peracchio, J.R. Izzo, Y. Hwu, F. De Carlo, W.K.S. Chiu, Journal of the Electrochemical Society 157 (2010) B783–B792.
[34] B. Münch, P. Gasser, R. Flatt, L. Holzer, Journal of the American Ceramic Society 89 (2006) 2586–2595.
[35] L. Holzer, B. Münch, Microscopy and Microanalysis 15 (2009) 130–146.
[36] J.C. Russ, The Image Processing Handbook, CRC Press, Boca Raton, USA, 1999.
[37] L. Holzer, B. Münch, M. Wegmann, R. Flatt, P. Gasser, Journal of the American Ceramic Society 89 (2006) 2577–2585.
[38] E.W. Washburn, Proceedings of the National Academy of Sciences, US, 1921, pp. 115–116.
[39] S. Diamond, Cement and Concrete Research 30 (2000) 1517–1525.
[40] L. Holzer, B. Muench, M. Rizzi, R. Wepf, P. Marschall, Applied Clay Science 47 (2010) 330–342.
[41] L. Holzer, B. Münch, B. Iwanschitz, M. Cantoni, T. Hocker, T. Graule, Journal of Power Sources (2010), doi:10.1016/j.jpowsour.2010.08.006.
[42] L. Holzer, F. Indutnyi, P. Gasser, B. Münch, M. Wegmann, Journal of Microscopy 216 (2004) 84–95.